DECEMBER 1996 ECN-I--96-060

BENDING-TORSION COUPLING OF A WIND TURBINE ROTOR BLADE

H.J.T. KOOIJMAN

Preface

This report is the third issue in the Smart Rotor project of ECN on the application of aeroelastic tailoring in rotor blades for horizontal axis wind turbines.
The first of two previous reports is a feasibility study released in March 1996 [ref. 11]. The second report, among others, contains a literature study on power regulation mechanisms of (historical) WECS and has been released in June 1996 [ref. 12].
This third report can best be considered as a scoping analysis on bending-torsion coupling of a wind turbine rotor blade through aeroelastic tailoring.
It also serves as a thesis work for the Faculty of Aerospace Engineering of the TUD. The aim has therefore been to make it also understandable by those who are not familiar with the nomenclature of wind turbine engineering. Nonetheless, for a more thorough understanding on some of the discussed aspects on wind power conversion the consultancy of other handbooks may be necessary [e.g. Spera, ref. 17].

The author wishes to thank his tutors at ECN and TUD, ir. Bernard Bulder and ir. Michel van Tooren respectively, for their assistance and useful advices. Also many thanks to the employees at the section wind energy of ECN for freely offering me their time and expertise, naming Jos Dekker, Koert Lindenburg, Gerard Schepers and Herman Snel.

Symbols

a	Axial induction factor = $V_{induced}$ / V	-
α	Effective angle of attack	°
β	Local pre-twist of the considered section, positive when decreasing the effective angle of attack (nose down)	°
ε_x	Longitudinal strain	-
ε_y	Transverse strain	-
ε_{xy}	Shear strain	-
ε_z	Total axial strain	-
η	Efficiency of energy conversion (drive train)	-
θ	Torsional deformation, positive when increasing the effective angle of attack (nose up)	°
κ_x	Change in curvature around the x-axis	1/m
κ_y	Change in curvature around the y-axis	1/m
κ_{xy}	Twist curvature	1/m
λ_r	Relative tip speed ratio = $\Omega \cdot r/V$ (r=R refers to blade tip span)	-
ρ	Air density	kg/m^3
σ	Stress or	N/m^2
	Solidity of a rotor ring = $(B \cdot c)/(2\pi r)$	-
υ	Poisson ratio	
Ω	Rotor rotational speed	rad/s
φ	Aerodynamic inflow angle w.r.t. the rotor plane $\varphi = \alpha + \beta$	°
a	Axial induction factor, actual axial inflow speed = $V_{wind}(1-a)$	-
B	Number of rotor blades	-
B_m	Induced twist per unit flatwise bending moment	m/N
B_s	Induced twist per maximum axial strain	-
c	Chord of the blade element	m
$c_{aver.}$	Average chord length of the blade element	m
$\bar{c}$	Effective chord length of a tapered blade element	m
c_d	Aerodynamic drag coefficient of the profile	-
c_l	Aerodynamic lift coefficient of the profile	-
c_m	Aerodynamic moment coefficient	-
Cp_i	Aerodynamic power coefficient, "i" refers to blade element number	-
dD	Drag force on a blade element	N
D	Flatwise shear force, positive in y-direction ("up wind")	N
$\{f\}$	(1×4) matrix with loads acting on the cross section	
dL	Lift force on a blade element	N
dr	Width of a blade element	m
E	Young's modulus of elasticity	N/m^2
EI	Bending stiffness of a cross section	Nm^2
G	Shear stiffness modulus	N/m^2
GJ	Torsional stiffness of a cross section	Nm^2
h	Height of the profile	m
i	Index number of a blade element	-
k	Weibull shape parameter to describe the wind speed distribution	-
M	Moment force on a blade element	Nm
P	(Aerodynamic) power	N·m/s
r	Span coordinate of a blade element	m
Q_{ij}	Specific laminate stiffnesses	N/m^2
R	Radius of the rotor blade	m

t	Thickness of the skin laminate	m
T	Operational time period of turbine for energy yield calculation	s
V	Wind speed	m/s
V_{ci}	Cut in wind speed, enough potential net electric power generation	m/s
V_{co}	Cut out wind speed, extreme condition stop	m/s
V_{rated}	Wind speed at which the turbine reaches nominal generator power	m/s
W	Effective wind speed on the blade element	m/s
x, y, z	Blade element chord reference system, chordwise-, flatwise- and radial direction respectively	m

Abbreviations and acronyms

ECN	Netherlands Energy Research Foundation ECN
FRP	Fibre Reinforced Polymers (also used is - Plastics)
HAWT	Horizontal Axis Wind Turbine
MATEC	Mechanical Analysis Tool for Elastic Cross sections
PHATAS	Programme for Horizontal Axis wind Turbine Analysis and Simulation
PVOPT	Power Wind speed OPTimization
TUD	Delft University of Technology
WECS	Wind Energy Conversion System

Laminate analogy

AFRP	Aramide Fibre Reinforced Polymer
CFRP	Carbon Fibre Reinforced Polymer
GFRP	Glass Fibre Reinforced Polymer
ca	Carbon fibre
gl	E-glass fibre
ep	Epoxy resin
s	Symmetrical laminate lay up w.r.t. midplane of the laminate
$[34_{ca}]_s$	Unidirectional carbon fibre, 34 degrees off axis with the principal material axis and symmetrical lay up.

ABSTRACT

With the increasing size of modern wind turbines the torsional deformation of rotor blades becomes more and more important in relation to aerodynamic power generation and blade stability. The shift from the conventional approach of increasing the torsional stiffness to the use of aeroelastic tailoring of Fibre Reinforced Plastics to **control limited torsional deformation** is a promising new way to improve rotor blade design.
The main objective of this study has been to develop an analysis for passive torsional deformation of a wind turbine rotor blade, in casu realised with a material coupling between flapwise bending and elastic twist of a constant speed rotor blade.

The relation between out of plane bending and torsional deformation due to an altered aerodynamic loading, c.q. wind speed variation, has been quantitatively studied for a virtual wind turbine model. By means of aeroelastic tailoring an unconventional **passive** coupling is created between flatwise bending and torsional deformation towards stall of the outer 60% of the blade span with a so called "mirrored lay up" of the suction and pressure side. Consequently the power curve is improved for wind speeds below rated value, which gives a potential increase in annual energy yield of several percentages, depending on the wind regime, control regulation method and chosen chord distribution of the rotor blade.

In order to induce the elastic twist a certain amount of bending-torsion flexibility must be implemented in the skin laminate. For a quantitative analysis of the structural (coupling) stiffnesses of a rotor blade element, a computer programme has been developed based on the coupling theory for a thin walled monocoque structure as described by Dr. N.M. Karaolis [ref. 9]. The input variables are the characteristic length of the element, its geometrical shape - including webs - and the extensional stiffnesses of the laminate ("A-matrix") which is used for the blade skin and web.
It has been shown that the bending-torsion flexibility - as required for optimum power generation below rated wind speed - can be achieved, preferably with an hybrid laminate lay up of carbon - and glass epoxy.
Carbon fibre induces the shear strain for torsion coupling, glass fibres on the other hand provide additional strength in other directions.

Important usage for the analysis has been made of the ECN programme PHATAS [ref. 13 and 14]. Recently the feature of coupling between implied loading (including other than flatwise bending) and elastic twist has been implemented in the PHATAS programme environment, thanks to the work of C. Lindenburg. Further attention must be paid to the modelling of opposite coupling between twist and bending in the computer programme.
Due to bending-torsion coupling towards stall the flexural axis is rotated aft of the shear centre line of the blade. Due to downwind bending the angles of attack of the blade elements increase. Despite an increase in aerodynamic damping, the reduction in aerodynamic stiffness predominates ("wash in"). Preliminary calculations have shown that because of this, below stall the dynamic stability of the blade is reduced.
Bending-torsion coupling towards feathering on the other hand, is expected to improve blade stability.

Elastic blade twist must be considered as an extra parameter for future blade design. Recommendations for further activities are:

- Research on the aerodynamic explanation for the required variation in blade twist to optimize power generation below rated wind speed. It has been found that for an optimum power generation below rated wind speed the elastic twist is typically towards feathering for the inner 40% of the blade span and, opposite, towards stall for the outer blade elements.
- Research on the dynamic flapwise stability in relation to bending-torsion coupling. Coupling towards feathering, e.g. applied with a flexbeam, may be an instrument to reduce the fatigue loading intensity of the blade.
- The implementation of torsional deformation and torsion-coupling mechanisms in future blade design, both in relation to power performance and stability aspects. This is specifically useful for larger wind turbines [Weber, ref. 20].

1. INTRODUCTION

The term "aeroelastic tailoring" is used to describe the design process that considers the effects of (intended) anisotropic mechanical properties of the structure to control aeroelastic deformation, either static or dynamic.
Most modern rotor blades are made of Fibre Reinforced Plastics (FRP) with a high torsion stiffness.
Already many research has been done by the Netherlands Energy Research Foundation ECN on flexibility of (part of) wind energy conversion systems, e.g. in the extensive FLEXHAT programme. This study specifically treats the concept of controlled torsional deformation of a wind turbine rotor blade by means of a built-in (aeroelastic) coupling between flapwise curvature and torsional deformation of the rotor blade.
The name Smart Rotor refers to an ECN research programme with the objective to develop a rotor which controls the aerodynamic power generation and reduces the internal loads of the rotor *without adding active systems*.

A virtual wind turbine model has been defined with a constant rotor speed and passive bending-torsion coupling of the blades; "Smart Rotor". The objectives of this study are:
- the formulation of a quantitative analysis for variable twist distribution of a rotor blade;
- to investigate the beneficial use of torsion coupling to enhance power generation below rated wind speed and
- to investigate specific design aspects in relation to bending-torsion coupling, e.g. production and stability of the blade.

This report does not present an optimized, applicable rotor design. By illustrating the opportunities of aeroelastic tailoring and giving a preliminary design analysis, it hopes though to encourage and support its application for future rotor blade designs.

The structure of the report is as follows.
First of all, in chapter 2 the studied virtual turbine model is described and the purpose of blade torsional deformation and the principle of aeroelastic tailoring are described.
Next in chapter 3 the quantitative analysis method for closed cross section profiles with possible anisotropic properties is described, hereby following the work of N.M. Karaolis [ref. 9].
Chapter 4 describes how the optimum twist deformation and geometry of the blade of the constant speed rotor have been determined.
By calculating the proportion of this elastic twist with the variation in loads the desired values for bending-torsion flexibility are derived; Chapter 5.
The materialization of those flexibilities in the structure is described in chapter 6, including an investigation of the influence of variations in laminate and geometry properties. Consequently, an appropriate design choice is made for the skin laminate, after which the mechanical properties are compared with the desired values from chapter 5.
Chapter 7 discusses some of the specific design aspects for rotor blades with torsion coupling, e.g. the rotation of the flexural axis.
Finally, chapter 8 gives preliminary information on the dynamic behaviour of a rotor blade with bending-torsion coupling including the last computer calculations on this subject.

The report ends with conclusions and recommendations and a number of appendices.

2. WIND TURBINE MODEL DESCRIPTION

2.1 Introduction

First in § 2.2 the essential characteristics of the turbine model are presented. Next in § 2.3 the basic principles of torsion coupling through aeroelastic tailoring are explained. The purpose of limited torsional deformation is explained in § 2.4 and more specified for bending-torsion coupling in § 2.5.

2.2 Basic properties of the Smart Rotor

For research purposes a virtual wind turbine model has been defined as a basis for the (computer) calculations; "Smart Rotor". The model is based on an existing 1 MW wind turbine. The main rotor characteristics are:

- a constant clockwise rotational speed of 24.6 revolutions per minute. The power variation is determined by the integration of the torque (M_t) on a rotor ring element; $P = \int_0^R \Omega \, dM_t$
- up wind configuration, i.e. the rotor is in front of the tower during normal operation;
- 3 flexible rotor blades with built-in aeroelastic bending-torsion coupling;
- 52.6 m diameter (2173 m^2 swept area);
- the main aerodynamic blade lies between 5.25 and 26.3 m span distances, consists of NACA 636 and 646 profile series.
- active stall regulation;
- 1.5 MW nominal power at a wind speed of $V_{rated} \approx 13.5$ m/s;
- cut in - and cut out wind speed are 4 and 25 m/s respectively.

The overall properties of the turbine are defined in a PHATAS model file as given in appendix A, which is generated after invoking a PHATAS calculation. [PHATAS: ref. 13 and 14].

2.3 Aeroelastic tailoring, torsion coupling principle

The use of Fibre Reinforced Plastics (FRP) has mostly been concentrated on strength optimization of a (rotor blade) construction. The present study moreover concentrates on optimizing the aeroelastic deformation of the blade, both to improve power generation as well as to control blade stability.

A lot of research has been carried out on the use of aeroelastic tailoring, mainly in the field of aerospace engineering. One well known example is the forward swept wing design for the Grumman X-29 Research Aircraft to improve the manoeuvrability [Weisshaar, ref. 21]. The enhanced danger of divergence due to wash-in was suppressed by rotating the elastic axis forward in front of the aerodynamic centres, by means of coupling bending and torsional deformation of the wing.

Figure 1 gives a qualitative impression of two important torsion-coupling mechanisms.

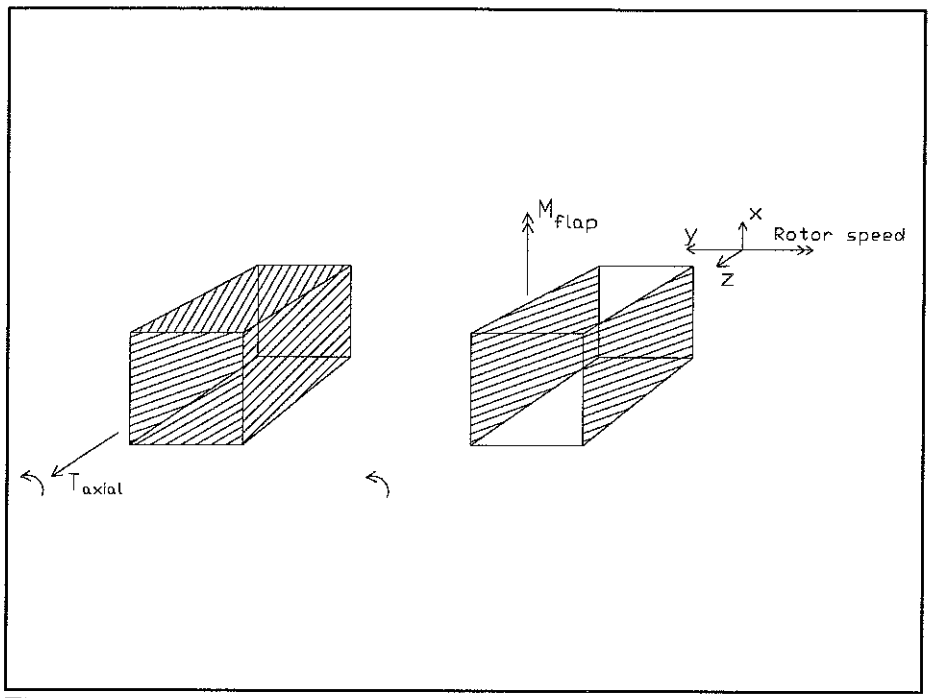

Figure 1: Tension-torsion and bending-torsion coupling respectively.

First is tension-torsion coupling of a construction with a helical winded lay up, also referred to as Circumferentially Uniform Stiffness distribution (CUS). An axial load will, besides an axial strain, also induce a torsional deformation of the structure at the free end.
Secondly, a bending-torsion coupling of the blade can be created by means of a mirror lay up w.r.t to the midplane of the section, also referred to as Circumferentially Asymmetric Stiffness (CAS). The laminate in itself will be unbalanced and (preferably) symmetric.

2.4 Why torsion coupling of a rotor blade?

The power generation of a rotor blade is often described with the so called $C_p(\lambda)$-relation according to blade element momentum theory:

$$P = C_P \cdot \frac{1}{2}\rho V^3 \pi R^2 \qquad [W]$$
$$\lambda = \frac{\Omega R}{V} \qquad [-] \qquad (2)$$

A maximum value of C_p can be maintained by adjusting the rotor speed such that $\lambda = \lambda_{opt.} \approx$ constant. Another variable for power generation is the pitch setting of the entire blade. Blade pitch regulation is normally used for limitation of aerodynamic power generation above rated wind speed and rarely applied for power control below rated.
The general idea of the present study is to use variable blade twist distribution to improve the effective $C_p(V)$-relation of a *constant speed rotor* for wind speeds below rated value. This should be realised by means of a passive coupling between imposed flatwise bending and induced twist for each blade element as described in figure 1.

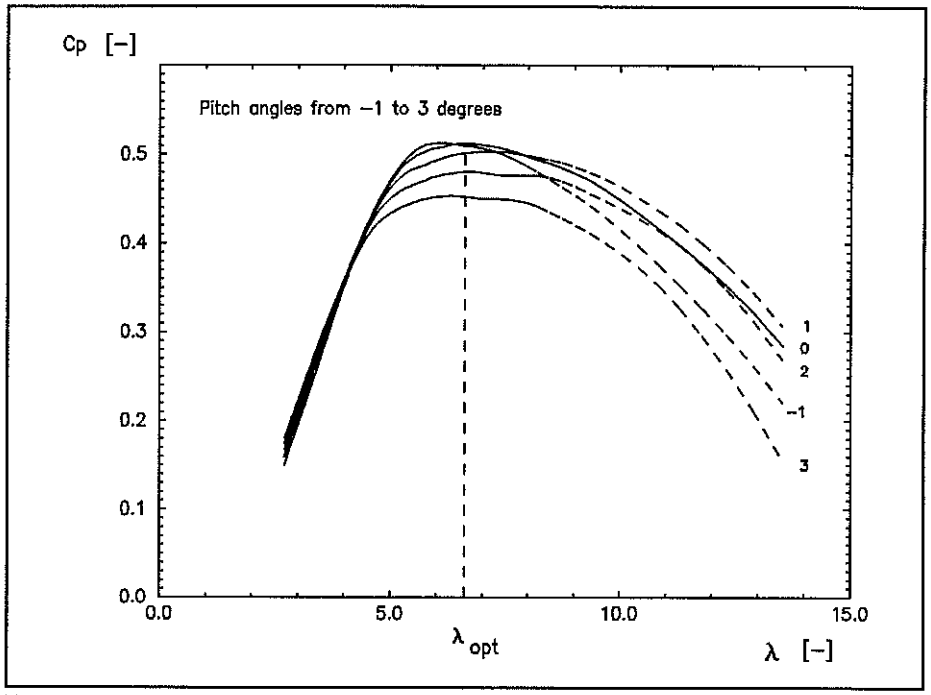

Figure 2: Power coefficient of the blade as a function of the relative rotor speed.

Energy yield of a turbine over a period (T) can be determined by a multiplication of T with a frequency distribution f(V) and the power generated at that specific wind speed; equation (3).

$$E = T \int_{V_{ci}}^{V_{co}} \eta \cdot P_{aero}(V)\, f(V)\, dV \qquad [J] \tag{3}$$

This implies that for a constant speed rotor the $C_p(V)$ line, see figure (2), is essential for energy yield.

The twist angle (β) directly influences the "effective angle of attack" (α) between blade chord and effective wind speed (W) and consequently the aerodynamic lift and drag force on the blade element.
The optimum relation between twist distribution and wind speed of the Smart Rotor blade is described in chapter 4.

2.5 Why bending-torsion coupling of a rotor blade?

Depending on the acting wind speed the rotor speed should be such that the effective angle of attack, and hence power generation, are optimal at every wind speed. This can be achieved when a constant λ control is applied. A disadvantage when compared to constant rotor speed, is the necessity of a converter system to transfer a constant voltage frequency on to the grid. A logical choice is to combine the opportunity of twist adjustment, to improve power generation, with constant rotor speed to maintain the advantages of a lighter gearbox and simple generator system.

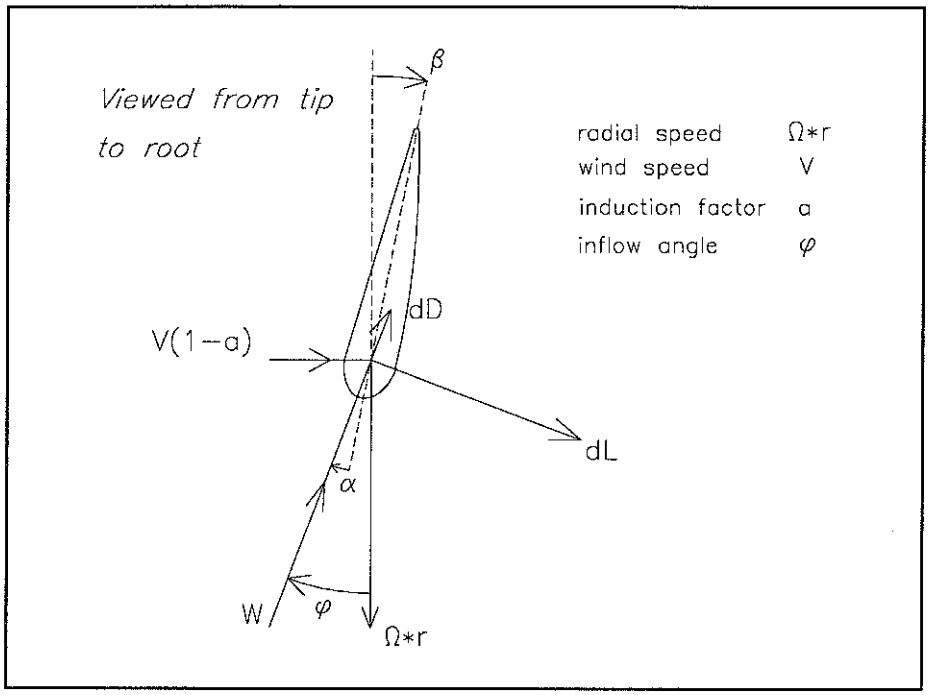

Figure 3: Aerodynamic characteristics of a blade element.

Bending-torsion coupling of a constant speed rotor blade enables the implementation of up-to-date design drivers as simplicity and reliability of the rotor. Main objective is to alter the laminate composition to improve the cost effectiveness of the rotor, without adding any additional mechanisms or systems.

Any wind speed variation will alter the aerodynamic bending moment and induce bending-torsion coupling. Variations in wind speed can be either deterministic, such as from tower influence or wind shear[1], or stochastic in the rotor plane itself. Whatever the origin of wind speed variation, passive bending-torsion coupling of the blade occurs.
Tension-torsion coupling however depends on the rotor rotational speed. Consequently, the stochastic wind speed variations in the rotor plane, acting on an individual blade, will not necessarily give an axial force in the blade and corresponding torsional coupling.

Several studies and applications have been carried out on passive power control by means of tension-torsion coupling, e.g. by SPE [ref. 3 and 4] and Karaolis [ref. 9 and 10].

[1] Distribution of wind speed in the rotor plane is quasi hyperbolic, i.e. the average wind speed acting on the blade tip when pointing downwards is less than when positioned vertically upwards. This wind shear effect increases for larger rotor diameters.

3. LAMINATE COUPLING THEORY ACCORDING TO KARAOLIS

3.1 Introduction

This chapter presents a method for qualitative analysis of torsion coupling. In a thesis called "The design of fibre reinforced composite blades for passive and active wind turbine aerodynamic control" [ref. 9], Dr. N.M. Karaolis formulated the stiffness properties of an arbitrary shaped, thin-walled profile. With a 4×4 stiffness matrix the relation between axial strain, 2 bending curvatures and torsional deformation of the section is related to the applied loads. The cross sectional stiffness matrix should be representative for a blade element with finite length.
The torsional deformation is obtained by combining the (bending) loads and stiffness matrix for several radial positions and than summating the induced twist along the span.
The essence of Karaolis' work has been analytically verified. Besides transformation of the equations to a right handed axis system also some noticeable corrections have been made which are here indicated by '!'. Other parts are, under appreciation, integrally copied from Karaolis' thesis.

3.2 Coupling theory for rotor blades

Classical lamination theory [Jones, ref. 8] gives for the stress-strain relation of a thin plate:

$$\begin{pmatrix} \epsilon_x \\ \epsilon_y \\ \gamma_{xy} \\ \kappa_x \\ \kappa_y \\ \kappa_{xy} \end{pmatrix} = \begin{bmatrix} a_{11} & a_{12} & a_{16} & b_{11} & b_{12} & b_{16} \\ a_{21} & a_{22} & a_{26} & b_{21} & b_{22} & b_{26} \\ a_{61} & a_{62} & a_{66} & b_{61} & b_{62} & b_{66} \\ b_{11} & b_{12} & b_{16} & d_{11} & d_{12} & d_{16} \\ b_{21} & b_{22} & b_{26} & d_{21} & d_{22} & d_{26} \\ b_{61} & b_{62} & b_{66} & d_{61} & d_{62} & d_{66} \end{bmatrix} \cdot \begin{pmatrix} N_x \\ N_y \\ N_{xy} \\ M_x \\ M_y \\ M_{xy} \end{pmatrix} \tag{4}$$

Similarly, the inverse relation between loads and strain is written in capital A, B and D.
N and M are 3×1-matrices containing the forces and moments per unit width in the laminate axis. ε and κ are the corresponding midplane strains and curvature vectors. A_{ij} is known as the extensional stiffness matrix since it relates in-plane forces to in-plane strains. D_{ij} is a bending stiffness matrix because it relates out of plane moments to curvatures. Matrix B_{ij} couples extensional loads with out of plane curvatures and vice-versa. For this reason B_{ij} is termed the coupling matrix.
More information on classical lamination theory, e.g. on the definition of the matrix elements, can be found in various handbooks, for example from Tsai [ref. 19] and Spies [ref. 18].

The following assumptions are made by Karaolis to derive the profile stiffness matrix from classical lamination theory:

- The blade cross section is treated as a thin walled beam structure (t<<c), which means that in-plane skin bending and - coupling are negligible w.r.t. the performance of the beam as a whole. Consequently κ is negligible. For a symmetrical lay up $[B_{ij}] = 0$ by definition.
- Only elastic deformations are considered.
- Stress concentrations, e.g. due to warping incompatibility or shear lag, are ignored [2].

In fact, the coupling between bending moments and torsional deformation of the cross section is due to coupling between in plane axial stress and shear strain of the skin laminate. Hence the [A] matrix suffices for the present analysis.

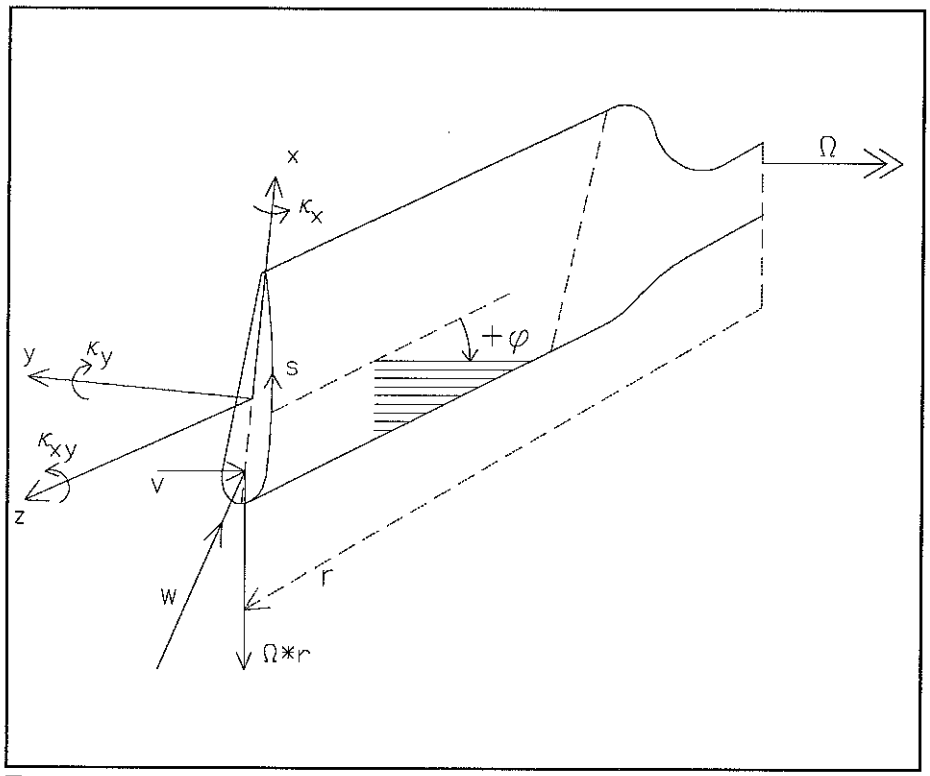

Figure 4: Nomenclature and positive directions for rotor blade analysis.

The fibre orientation (φ) is measured with respect to the z-axis and is taken positive in the quadrant defined by the positive z- and s-directions. In figure 4, $+\varphi$ is depicted in the negative z and negative s direction.

---

[2] An argument in favour of the use of Karaolis' theory for this study is its application for the outer, slender, part of the rotor blade, as later will be explained.
A somewhat more sophisticated model is described by Armanios and Badir [ref. 2]. Different from Karaolis, an additional function g(s,x) is added to the classical displacement function (equation (8)), which represents the out of plane warping of the cross section. Nevertheless, when expressed in terms of A_{ij} and geometry variables, the ultimately derived expressions for the stiffness relations [4x4] are identical to these formulated in equations (16) and (17) !

Positive torsional deformation corresponds to a decrease in pitch angle (β). Hence, the total pitch angle ($\beta(r)$) of an element between chord and rotor plane is defined as the summation of blade pitch angle (β_{pitch}), the constant twist of the element (β_{twist}) and the torsional deformation or elastic twist (θ):

$$\beta(r) = \beta_{pitch}(R) + \beta_{twist}(r) - \theta(r) \tag{5}$$

The pitch angle is defined at the blade tip. Here, the blade pitch angle is defined at 0°, unless stated otherwise. Thus, for zero blade pitch, the actual pitch angle of each element is the same as the total twist.

Using equation (3) and the nomenclature from figure (4) gives the skin stiffness matrix ($A_{61} = A_{31}$, etc.):

$$\begin{Bmatrix} N_z \\ N_s \\ N_{zs} \end{Bmatrix} = \begin{bmatrix} A_{11} & A_{12} & A_{13} \\ A_{21} & A_{22} & A_{23} \\ A_{31} & A_{32} & A_{33} \end{bmatrix} \begin{Bmatrix} \varepsilon_z \\ \varepsilon_s \\ \gamma_{zs} \end{Bmatrix} \tag{6}$$

In which N_z is the longitudinal or axial load and N_{zs} the shear load, both per unit width; [N/m]. Because no internal pressure, nor restraint due to a Poisson effect is considered, N_s=0.

Note: A distinction must be made between loads in the rotor plane axis system, namely "flap-" and "lagwise" bending, and those in the local chord axis system, namely "flat-" and "edgewise" bending. The latter are used when analyzing the elastic deformation of a blade element.

The stiffness matrix can be written in terms of the ply thickness fraction t_k' by dividing by the total laminate thickness t:

$$t_k' = \frac{t_k}{t}$$
$$A_{ij} = \sum_{k=1}^{N} (Q_{ij})_k t_k' t = A_{ij}' t \qquad [N/m] \tag{7}$$

In the above and following equations, a prime indicates a dimensionless parameter, e.g. ds= c · ds′; A= c^2 · A′ or x= c · x′, etc.
Q_{ij} represents the elements of the stiffness matrix (of the k^{th} ply) which are functions of the elastic properties and fibre orientation of the individual plies.

The following expression is used to describe the deformation in the cross section of the blade (8):

$$\varepsilon_z(x,y) = \varepsilon_z^0 - x\,\kappa_y + y\,\kappa_x \tag{8}$$

For the shear stress in the skin, resulting from torsional moments on the cross section the following relation has been used:

$$N_{zs} = \frac{M_z}{2A} \tag{9}$$

By substitution of (8) and (9) in (6) and after some manipulation, axial load, shear strain and transverse strain can be derived:

$$N_z = S_1 t(\varepsilon_z^0 - x'c\kappa_y + y'c\kappa_x) - S_2 \frac{M_z}{2A'c^2}$$

$$\gamma_{zs} = S_2(\varepsilon_z^0 - x'c\kappa_y + y'c\kappa_x) + \frac{S_3}{t}\frac{M_z}{2A'c^2} \qquad \textbf{(10)}$$

$$\varepsilon_s = S_4(\varepsilon_z^0 - x'c\kappa_y + y'c\kappa_x) + \frac{S_5}{t}\frac{M_z}{2A'c^2}$$

In which S_i (i = 1, 2, .., 5) are stiffness parameters in terms of A_{ij}[3] :

$$S_1 = A'_{11} + \frac{2A'_{12}A'_{13}A'_{23} - A'^2_{12}A'_{33} - A'^2_{13}A'_{22}}{A'_{22}A'_{33} - A'^2_{23}} \quad !$$

$$S_2 = \frac{A'_{12}A'_{23} - A'_{13}A'_{22}}{A'_{22}A'_{33} - A'^2_{23}} \qquad S_3 = \frac{A'_{22}}{A'_{22}A'_{33} - A'^2_{23}} \qquad \textbf{(11)}$$

$$S_4 = \frac{A'_{13}A'_{23} - A'_{12}A'_{33}}{A'_{22}A'_{33} - A'^2_{23}} \quad ! \qquad S_5 = \frac{-A_{23}'}{A'_{22}A'_{33} - A'^2_{23}}$$

S_2 and S_4 are dimensionless, whereas S_1 has dimensions N/m^2 and S_3 and S_5 are in terms of m^2/N. The sign of the parameters S_2 and S_5 depends on the sign of the fibre orientation which governs the sign of the matrix elements A_{13} and A_{23}. The sign of S_1 and S_3 is always positive.

The actual external forces acting on the cross section are (equation 12)[4]:

$$T_z = c\oint N_z\, ds'$$
$$M_x = c^2\oint y' N_z\, ds' \qquad \textbf{(12)}$$
$$M_y = -c^2\oint x' N_z\, ds' \quad !$$

---

[3] Karaolis:

$$S_1 = A'_{11} + \frac{2A'_{12}A'_{13}A'_{23} - A'^2_{12}A'_{33} - A'^2_{13}A'_{23}}{A'_{22}A'_{33} - A'^2_{23}}$$

$$S_4 = \frac{A'_{12}A'_{23} - A'_{13}A'_{33}}{A'_{22}A'_{33} - A'^2_{23}}$$

[4] Karaolis:

$$M_y = +c^2\oint x' N_z\, ds'$$

Substitution of the equation for N_z from (10) in (12) gives the following expressions for respectively the axial force, flatwise and edgewise bending moments:

$$T_z = \varepsilon_z^o tcS_1 \oint ds' - k_y tc^2 S_1 \oint x'\,ds' + k_x tc^2 S_1 \oint y'\,ds' - \frac{M_z}{2A'c} \oint S_2 ds'$$

$$M_x = \varepsilon_z^o tc^2 S_1 \oint y'\,ds' - k_y tc^3 S_1 \oint x'y'\,ds' + k_x tc^3 S_1 \oint y'^2 ds' - \frac{M_z}{2A'} \oint y' S_2\,ds'$$

$$M_y = -\varepsilon_z tc^2 S_1 \oint x'\,ds' + k_y tc^3 S_1 \oint x'^2 ds' - k_x tc^3 S_1 \oint x'y'\,ds' + \frac{M_z}{2A'} \oint x' S_2 ds' \qquad \textbf{(13)}$$

S_2 is kept within the integral sign to account for changes in its sign that may occur along s, due to a possible change in sign of fibre orientation.

The shear strain γ_{zs} from (10) defines the torsion per unit length κ_{xy}[5]:

$$\kappa_{xy} = \frac{1}{2A} \oint^s \gamma_{zs} ds$$
$$= \frac{1}{2A'} \left[\frac{\varepsilon_z^0}{c} \oint S_2 ds' - \kappa_y \oint x' S_2 ds' + \kappa_x \oint y' S_2 ds' + \frac{M_z S_3}{2A' c^3 t} \oint ds' \right] \quad ! \qquad \textbf{(14)}$$

After rewriting this equation for M_z and substitution in (12) the *symmetric stiffness relation of the section* $[H_{ij}]$ is finally obtained as:

$$\begin{Bmatrix} T_z \\ M_x \\ M_y \\ M_z \end{Bmatrix} = \begin{bmatrix} H_{11} & H_{12} & H_{13} & H_{14} \\ H_{12} & H_{22} & H_{23} & H_{24} \\ H_{13} & H_{23} & H_{33} & H_{34} \\ H_{14} & H_{24} & H_{34} & H_{44} \end{bmatrix} \begin{Bmatrix} \varepsilon_z^0 \\ \kappa_x \\ \kappa_y \\ \kappa_{xy} \end{Bmatrix} \qquad \textbf{(15)}$$

The composition of the stiffness elements is described in equations (16). The dimensions of H_{1j} are: H_{11} in [N] and H_{12}, H_{13} and H_{14} in [Nm]. The other terms all in [Nm^2].

[5] Karaolis:

$$\kappa_{xy} = \frac{1}{2A'} \left[\frac{\varepsilon_z^0}{c} \oint S_2 ds' - \kappa_y c \oint x' S_2 ds' + \kappa_x c \oint y' S_2 ds' - \frac{M_z S_3}{2A' c^3 t} \oint ds' \right]$$

Alternatively, $[H^*_{ij}]$ is the *reduced stiffness matrix* of the considered blade section, independent of the dimensions t and c. The dimensions are all in $[N/m^2]$. Of course H^*_{ij} contains the information on the stiffness and coupling characteristics of the section, i.e. the laminate properties from equations (7) and (10)[6]:

$$\begin{Bmatrix} T_z \\ M_x \\ M_y \\ M_z \end{Bmatrix} = \begin{bmatrix} H^*_{11}tc & H^*_{12}tc^2 & H^*_{13}tc^2 & H^*_{14}tc^2 \\ H^*_{12}tc^2 & H^*_{22}tc^3 & H^*_{23}tc^3 & H^*_{24}tc^3 \\ H^*_{13}tc^2 & H^*_{23}tc^3 & H^*_{33}tc^3 & H^*_{34}tc^3 \\ H^*_{14}tc^2 & H^*_{24}tc^3 & H^*_{34}tc^3 & H^*_{44}tc^3 \end{bmatrix} \begin{Bmatrix} \varepsilon^0_z \\ \kappa_x \\ \kappa_y \\ \kappa_{xy} \end{Bmatrix} \qquad \textbf{(16)}$$

$$H^*_{11} = S_1 \oint ds' + \frac{\left[\oint S_2 ds'\right]^2}{S_3 \oint ds'} \qquad H^*_{12} = S_1 \oint y' ds' + \frac{\oint S_2 ds' \oint y' S_2 ds'}{S_3 \oint ds'}$$

$$H^*_{13} = -S_1 \oint x' ds' - \frac{\oint S_2 ds' \oint x' S_2 ds'}{S_3 \oint ds'} \qquad H^*_{14} = -2A' \frac{\oint S_2 ds'}{S_3 \oint ds'}$$

$$H^*_{22} = S_1 \oint y'^2 ds' + \frac{\left[\oint y' S_2 ds'\right]^2}{S_3 \oint ds'} \qquad H^*_{23} = -S_1 \oint y' x' ds' - \frac{\oint y' S_2 ds' \oint x' S_2 ds'}{S_3 \oint ds'}$$

$$H^*_{24} = -2A' \frac{\oint y' S_2 ds'}{S_3 \oint ds'} \qquad H^*_{33} = S_1 \oint x'^2 ds' + \frac{\left[\oint x' S_2 ds'\right]^2}{S_3 \oint ds'}$$

$$H^*_{34} = 2A' \frac{\oint x' S_2 ds'}{S_3 \oint ds'} \quad ! \qquad H^*_{44} = \frac{4A'^2}{S_3 \oint ds'} \qquad \textbf{(17)}$$

[6] Karaolis:

$$H^*_{34} = -2A' \frac{\oint x' S_2 ds'}{S_3 \oint ds'}$$

The flexibility matrix $[h_{ij}]$ is defined as the inverse of $[H_{ij}]$, viz. (18):

$$\{\varepsilon_{ij}\} = [h_{ij}]\ \{f_{ij}\}$$

$$[h_{ij}] = \begin{bmatrix} h_{11}^*/tc & h_{12}^*/tc^2 & h_{13}^*/tc^2 & h_{14}^*/tc^2 \\ h_{12}^*/tc^2 & h_{22}^*/tc^3 & h_{23}^*/tc^3 & h_{24}^*/tc^3 \\ h_{13}^*/tc^2 & h_{23}^*/tc^3 & h_{33}^*/tc^3 & h_{34}^*/tc^3 \\ h_{14}^*/tc^2 & h_{24}^*/tc^3 & h_{34}^*/tc^3 & h_{44}^*/tc^3 \end{bmatrix} \quad \textbf{(18)}$$

In which h^*_{ij} are all in $[m^2/N]$.
The amount of torsional deformation of a blade element,

$$\Delta\theta = \kappa_{xy} \cdot \Delta r \qquad [rad] \quad \textbf{(19)}$$

in general depends on:
- the properties of the extensional stiffness matrix, i.e. fibre orientations of the plies, fibre and matrix properties and thickness of the plies and laminate;
- the imposed axial strain, i.e. the thickness distribution in case of bending-torsion;
- the limitations due to strength or maximum strain criteria and
- the blade chord distribution, specifically taper.

More on the coupling performance of the Smart Rotor blade is given in chapter 5.

4. AERODYNAMIC OPTIMIZATION OF BLADE GEOMETRY

4.1 Introduction

The aim of the variable twist for wind speeds below rated value is to optimize the power generation of each blade element. Chapter 2 already described the concept of aerodynamic power generation and the definition of the twist angle. Chapter 3 described how the variable twist can be achieved by means of variation in aerodynamic (bending) loading on the blade. This chapter describes the aerodynamic design considerations to achieve an optimum annual energy yield of a rotor blade with torsional flexibility.

The Smart Rotor aerodynamic profiles are NACA 63-6 and 64-6 series; the same as are applied on the existing 1 MW turbine. Computer calculations have been carried out with the programme PVOPT [ref. 15] to investigate the optimum blade geometry of the Smart Rotor. PVOPT iteratively determines the optimum fixed blade twist and chord distribution resulting in maximum annual energy yield. Of course other cost factors are also relevant, but for the present study the "power curve optimization" suffices. The main input parameters in PVOPT are:

- average wind speed and Weibull parameter;
- nominal (generator) power;
- rotor speed;
- aerodynamic profile distribution and
- pitch regulation for power limitation above rated wind speed.

Unlike in the more sophisticated ECN programme for wind turbine simulation PHATAS (chapter 7), aeroelasticity is not considered in PVOPT. The results for blade chord and twist of the Smart Rotor blade are discussed in § 4.2 and § 4.3 respectively.
The result for the desired variation in blade twist is analytically investigated in § 4.4. Finally § 4.5 presents the chosen preliminary aerodynamic shape of the Smart Rotor blades followed by a presentation of the potential increase in energy yield (§ 4.6) and some practical considerations (§ 4.7).

The wind regime for the Smart Rotor study is described with an average wind speed of 8.0 m/s and Weibull shape parameter k=2.39; figure 5. Those values are obtained from wind speed measurements for a location near Medemblik (NL) and for 60.0 m height of the rotor hub [ref. 5].

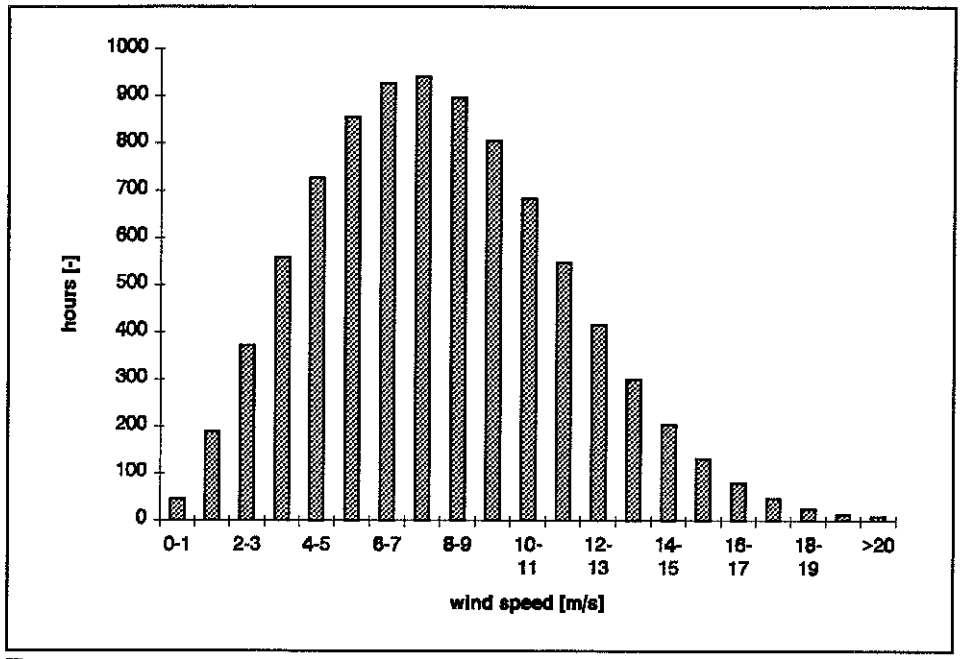

Figure 5: Representative wind speed distribution at 60 m hub height.

4.2 Optimum chord distribution

The unusual approach of assuming a variation in blade twist with the acting wind speed implies that the optimum planform of the blade should also be adjusted. Consequently, the optimum blade chord distribution for the entire wind regime has been determined for a constant twist distribution.
The optimum root chord will be limited at a maximum of 3.2 m because of fabrication and/or transportation aspects, slightly less than the theoretical optimum of approximately 3.4 m according to PVOPT. The chord distribution is linearly decreasing to $c_{tip} \approx 1$ m.
Three additional aspects to be considered in the planform design are:

- Parking loads for a tapered blade are less. This should be brought in relation with collision danger of blade tip and tower due to a possible decrease in flapwise bending stiffness.
- The induced torsion per flatwise bending load is proportional to $1/c^3$ (chapter 3). If needed, a high aspect ratio is favourable to increase the amount of elastic torsion.
- Aeroelastic stability of the blade, of which the relation with the planform lies beyond the scope of this study.

A more elaborate discussion on the influence of geometrical properties is given in chapter 5.

4.3 Optimum twist distribution

Figure 2 implicitly shows that for a maximum C_p of a constant speed rotor, the twist distribution of the blade should ideally vary with the acting wind speed. A change in optimum twist setting (β) of the element is determined by the change in aerodynamic inflow angle due to ΔV and the altered optimum effective angle of attack which determines the "lift over drag" - relation.

Both analytical expressions and computer simulations show for the (constant speed) Smart Rotor that with increasing wind speed:
- the inner blade elements require a positive twist (towards feathering) to compensate for the increase in effective angle of attack (α) and
- optimum aerodynamic power generation of the outer blade elements implies a negative twist adjustment (towards stall), hence intensifying the increase in effective angle of attack.

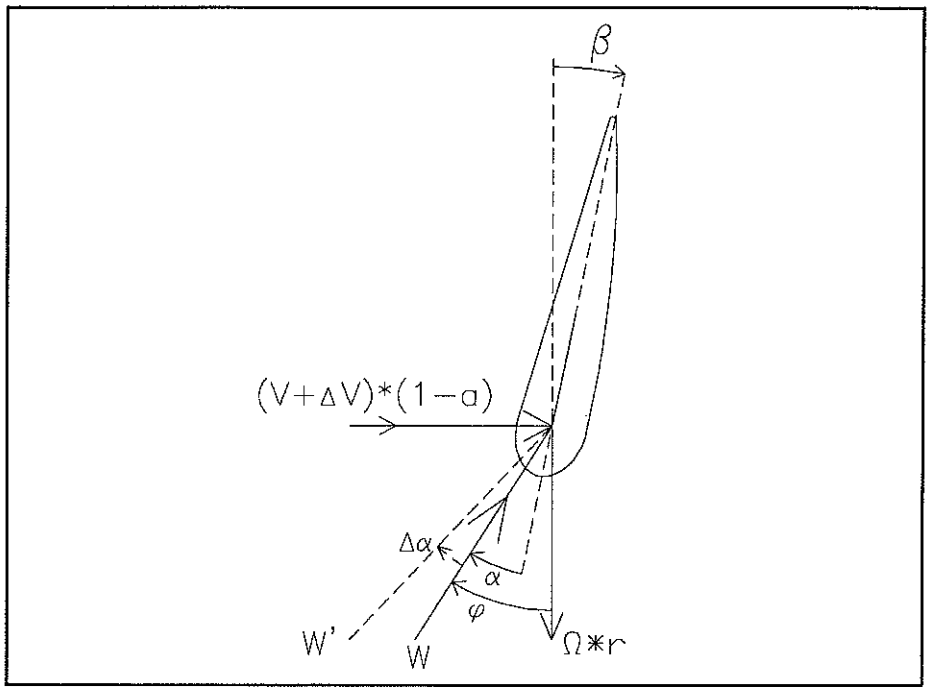

Figure 6: Change in angle of attack due to ΔV.

A better understanding of the desired twist of a blade element is found from the definition of the tangential force on a blade element:

$$F_{tang.} = (c_l \sin\varphi - c_d \cos\varphi) \cdot \frac{1}{2}\rho V^2 \bar{c}\, dr \qquad (20)$$

With increasing wind speed the inflow angle φ increases also (figure 3). Consequently $\cos(\varphi)$ in equation (20) decreases and there is a shift towards increasing angles of attack (and larger values of c_d and c_l) for a maximum tangential force.
If the direct increase in angle of attack due to ΔV is less than the required increase for a maximum tangential force as described above, an additional pitching towards stall is required:

$$\varphi = atan\left(\frac{V(1-a)}{\Omega \cdot r}\right) \qquad (21)$$

$$-\Delta\theta = \Delta\beta = \Delta\varphi - \Delta\alpha_{opt}$$

The phenomena of negative twist of especially the outer blade elements is confirmed by the fact that, due to the relatively larger radial speed, the increase in inflow angle with V is less.

The best individual twist distributions for average wind speeds of 5, 6, ... and 13 m/s have been determined. The procedure has been to define an extremely large Weibull scale parameter (k=8) for each wind speed, thereby defining a concentrated wind speed "distribution" (quasi discrete wind speed).

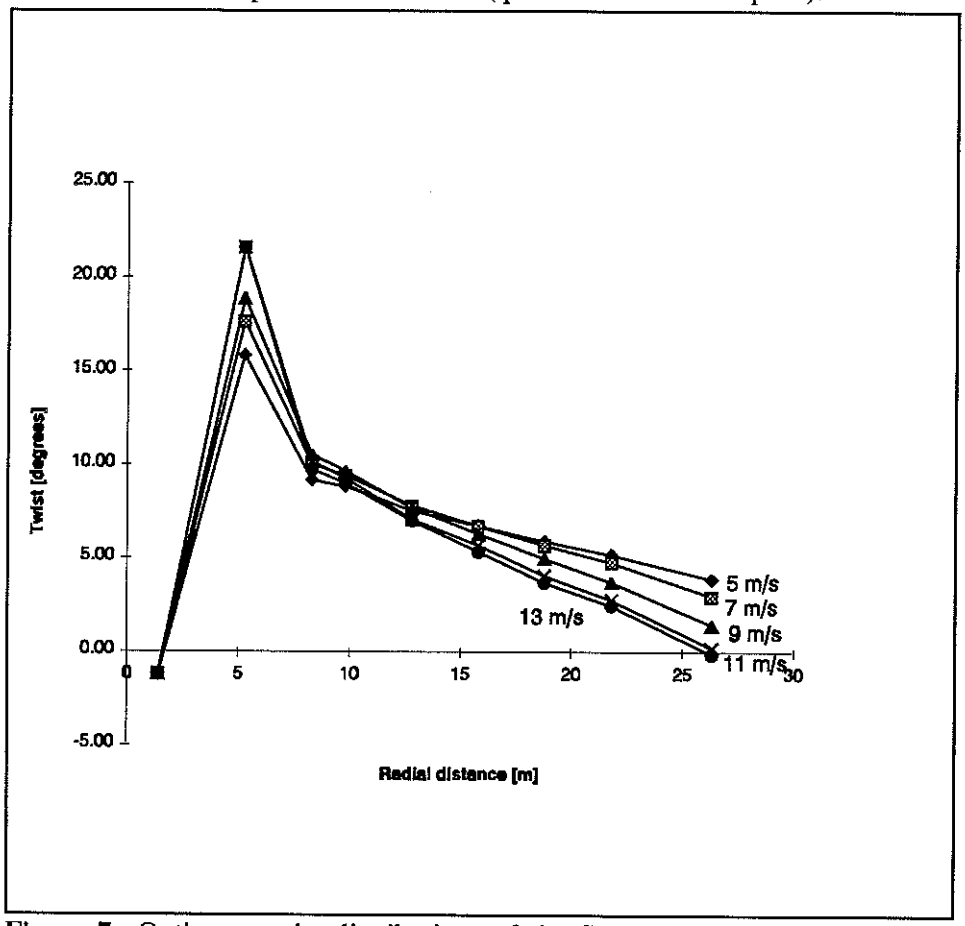

Figure 7: Optimum twist distributions of the Smart Rotor blade for various wind speeds below rated value (PVOPT).

Computer simulations for an other constant speed wind turbine (and other aerodynamic profiles) have shown the same qualitative behaviour (figure in appendix B).

The phenomenon that the direction in desired twist of a blade element depends on its radial position has also been verified with PHATAS calculations. To realise a maximum power coefficient of an element near the tip a negative pitch adjustment from +1° to -1° is derived (figure 8).
For a blade element around 9 m span distance however the potential improvement in power generation by means of adjusting the pitch setting is small (figure 9).

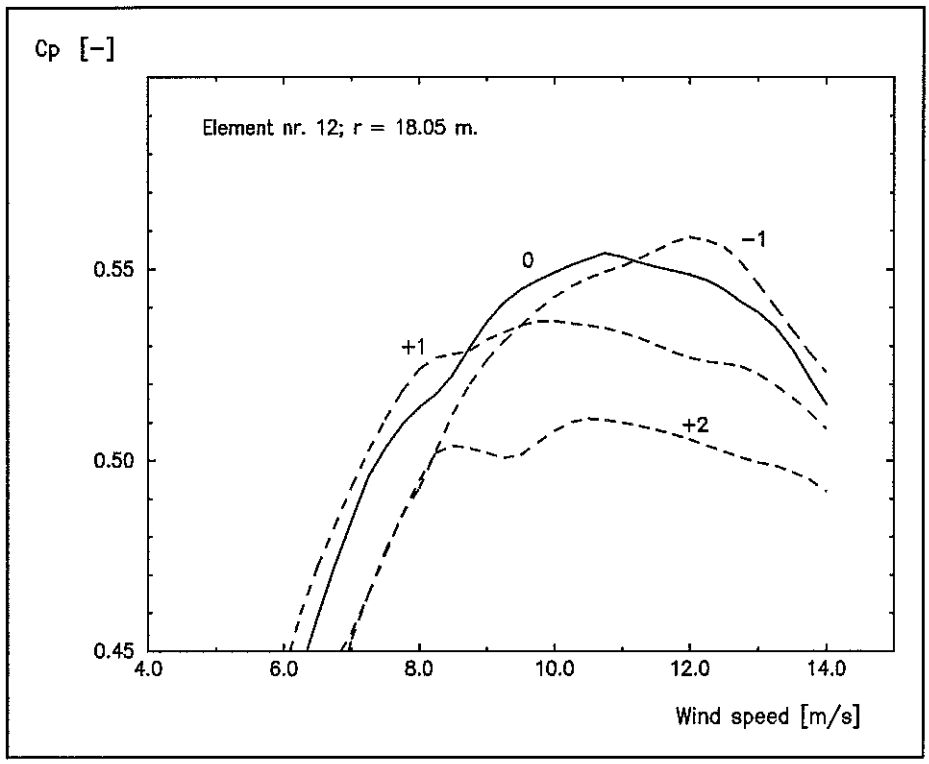

Figure 8: Maximum C_p when blade pitch regulation as +1° → 0° → -1° , i.e. increasing α (PHATAS).

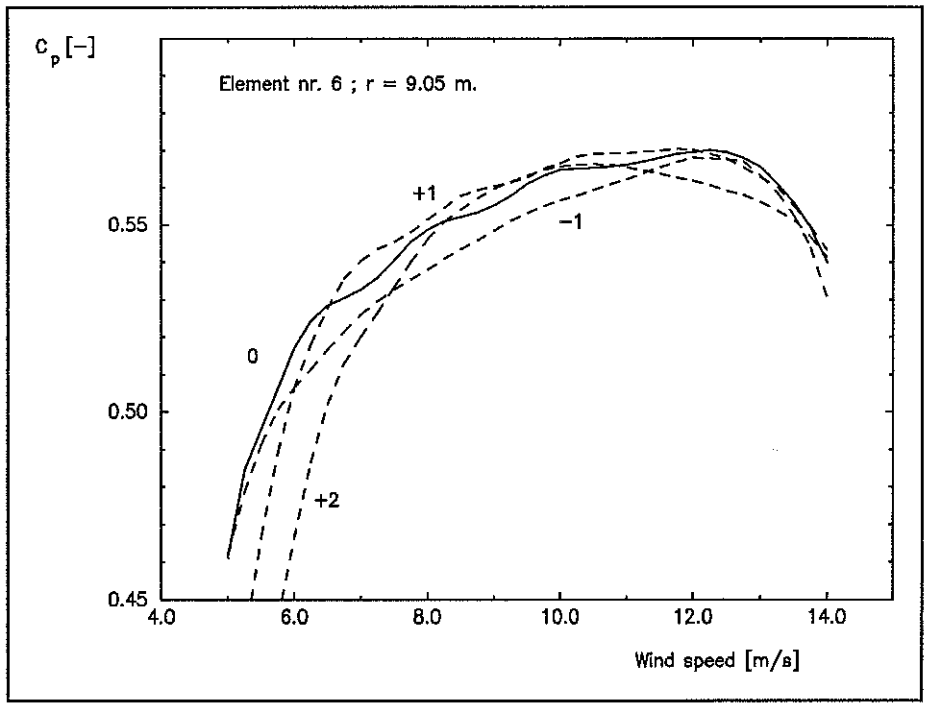

Figure 9: Maximum power coefficient for all wind speed is a blade pitch setting of approximately +1° (PHATAS).

4.4 Analytical explanation for optimum pitch setting of a blade element

The change in twist of a blade element with the wind speed, either negative or positive, is determined by the difference in alterations between inflow angle (φ) and the optimum value for the effective angle, i.e. a maximum power coefficient of the element.
The inflow angle is defined by:

$$\varphi = atan\left(\frac{V(1-a)}{\Omega \cdot r}\right) \tag{22}$$

Hence, the desired change in twist of an element is formulated as:

$$\beta_{V_1} - \beta_{V_2} = \left[atan\left(\frac{V_1(1-a_1)}{\Omega r}\right) - \alpha(opt)_{V_1}\right] - \left[atan\left(\frac{V_2(1-a_2)}{\Omega r}\right) - \alpha(opt)_{V_2}\right]$$

$$\Leftrightarrow \beta_{V_1} - \beta_{V_2} > 0 \quad \textit{(negative change of twist) only than if :} \tag{23}$$

$$\alpha(opt)_{V_2} - \alpha(opt)_{V_1} > atan\left(\frac{V_2(1-a_2)}{\Omega r}\right) - atan\left(\frac{V_1(1-a_1)}{\Omega r}\right)$$

This means that the sign in blade twist variation is determined by the difference in slope for α and φ with the wind speed (V).
For a qualitative analysis of α(V), an expression (22) has been derived for the optimum value of c_l / c_d as a function of (V), viz.:

$$\left(\frac{c_l}{c_d}\right)_{opt} = \frac{\lambda_r}{(1-a)} \cdot \frac{2+3\left(\frac{\lambda_r}{1-a}\right)^2}{1+2\left(\frac{\lambda_r}{1-a}\right)^2} \tag{24}$$

The equation is derived by a simplified formulation of the blade element power coefficient $C_p = C_p$ (λ_r, c_l, c_d, a), using blade element momentum theory. By equating the derivative of C_p to λ_r to zero and some manipulation equation (24) is derived. The axial induction factor (a) is considered to be constant. Appendix C gives a complete derivation of (24).

The expression for α_{opt}(V) can now be derived by comparing (24) with the (c_l/c_d) (α) from profile data.

An alternatively procedure to express λ_r in terms of φ and writing $C_p = C_p(\varphi)$ - thereby considering the other variables to be constant - gives a non continuous function which therefore can not be used to derive an expression for α_{opt}.

Example:
For the blade tip element (average radial distance = 24.05 m) the previously derived relation for $(c_l/c_d)_{opt}$ is plotted as a function of the wind speed, by substitution of the rotor speed Ω = 2.576 rad/s and the axial wind speed induction factor (a) $\approx$ ⅓.
Despite the differences in assumptions - specifically a constant axial induction factor and zero radial induction - figure (10) shows that in this case the slope for α_{opt} is more pronounced than that for φ and thus negative twist is desired for an optimum power coefficient with increasing wind speed.
The slope of the inflow angle with increasing wind speed will be less for blade elements near the blade tip, due to the relatively small radial speed vector ($\Omega \cdot r$). This basically explains why the direction of desired twist depends on the span distance of the blade element.
In order to have a negative twist for power optimization for blade element closer to the root as well, profiles are required with a high c_l/c_d ratio for angles of attack between c_l/c_d (max) and c_l(max). This will not be easy to realise because correspondent prolonged laminar flow, is already an existing design driver for rotor aerodynamics.

Difference between α and φ determines the desired twist variation.				
V [m/s]	λ [-]	c_l/c_d (opt) [-]	α [°] (opt)	φ [°]
6	10.33	23.1		3.7
7	8.85	19.8	14.0	4.3
8	7.75	17.4		4.9
9	6.88	15.44	15.4	5.5
10	6.20	13.9		6.1
11	5.63	12.6	16.8	6.8
12	5.16	11.6		7.4
13	4.77	10.7	18.0	8.0
14	4.43	10.0		8.6

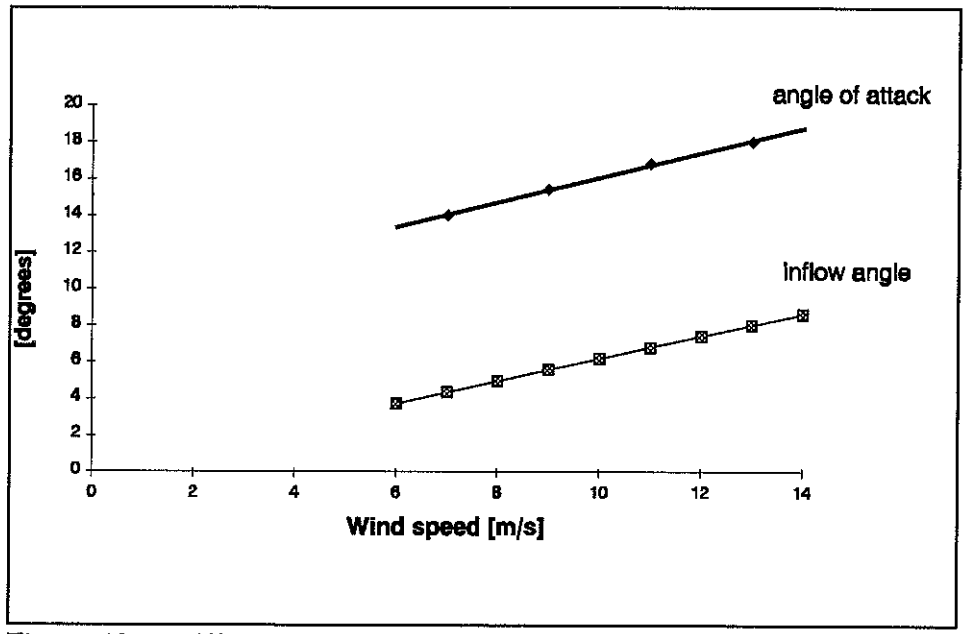

Figure 10: Difference in slope between α_{opt} and φ determines the change in twist for optimum C_p regulation.

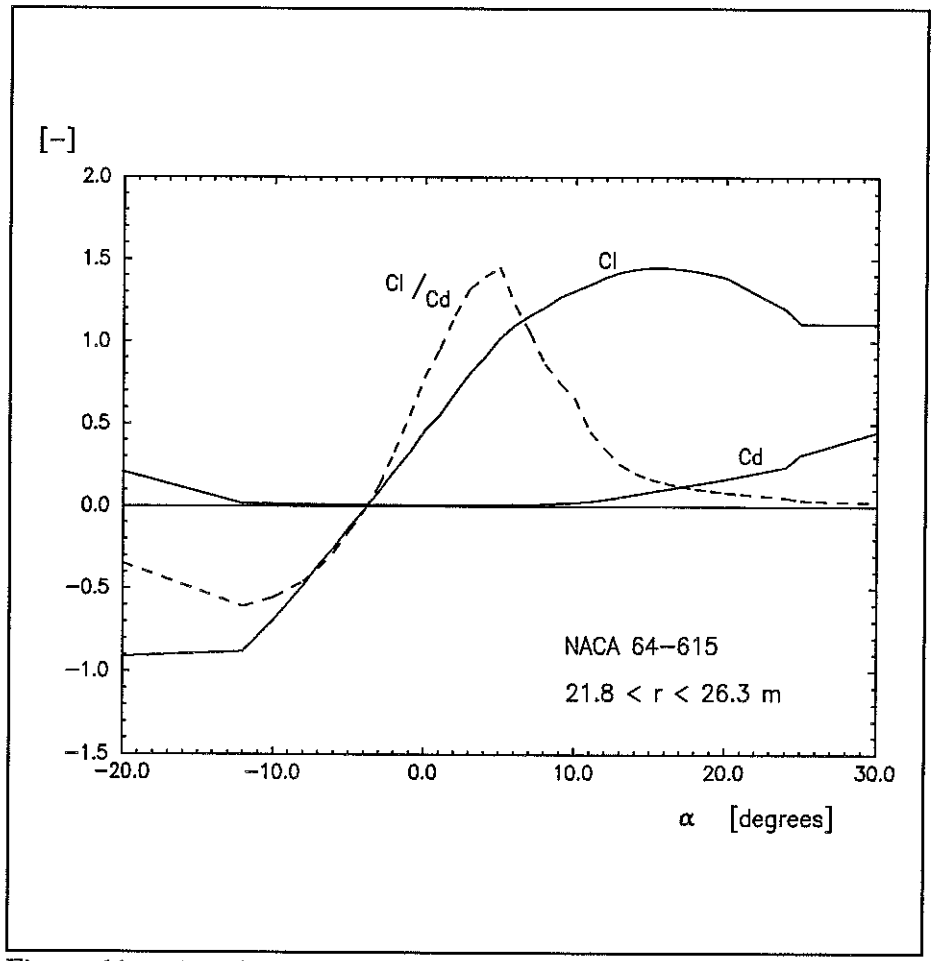

Figure 11: Aerodynamic profile data of the blade tip section elements.

4.5 Actual aerodynamic shape of the smart rotor blade

With increasing wind speed the desired twist of the outer blades is towards stall. For an optimum twist variation of the entire blade the opposite twist deformation of the inner blade elements towards feathering would mean an extreme unrealistic large torsional deformation of the outer blade elements in order to achieve the increase in effective angle of attack. Therefore only the outer blade - from 9.8 m radial distance to the tip - is supposed to have bending-torsion coupling. Consequently a new twist optimization for V = 5, 6, ... 13 m/s has been made with a twist variation of the outer blade and a constant twist distribution up to 9.8 m radial distance.

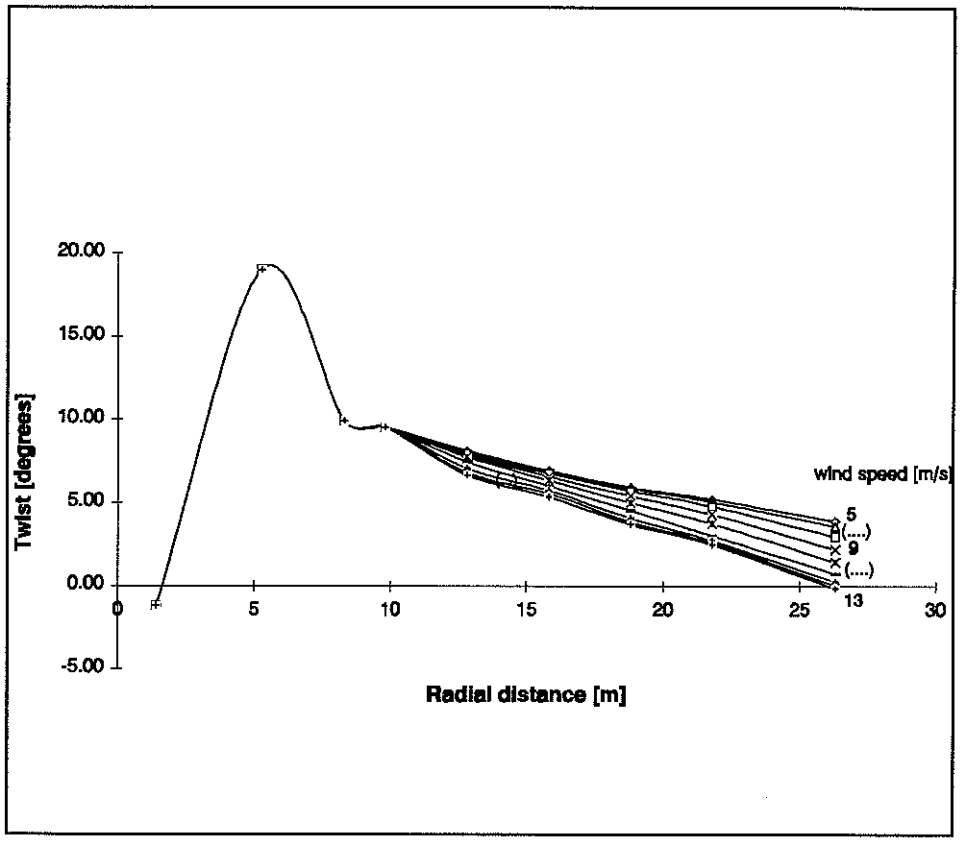

Figure 12: Optimum twist variation of the outer part of the Smart Rotor blade (PVOPT).

The corresponding numerical values for elastic twist variation are given in the table on the next page.

Ideal aerodynamic shape of the Smart Rotor blade (blade pitch = 0°)					
$r_{mid\ element}$ [m]	Δr [m]	NACA #	$c_{average}$ [m]	β_5(opt) [°]	β_{13}(opt) [°]
5.3	3.0	63627	2.96	18.99	18.99
8.3	3.0	63627	2.88	9.91	9.91
11.3	3.0	63621	2.57	8.47	8.16
14.3	3.0	63618	2.25	7.07	6.10
17.3	3.0	63618	1.94	6.33	4.54
20.3	3.0	64618	1.63	5.55	3.09
24.05	4.5	64615	1.24	4.57	1.16

4.6 Potential increase in energy yield

The following table shows an increase in generator capacity factor of something more than 1% when torsional deformation is applied for the Smart Rotor blade having an optimum planform.

			With torsion coupling:			*Without torsional deformation:*		
Wind speed			Power	Energy yield		Power	Energy yield	
Interval [m/s]	Relative %	Year [hours]	[kW]	[kWh]	%	[kW]	[kWh]	%
0-1	0.52	45.4						
1-2	2.17	189.8						
2-3	4.24	371.1						
3-4	6.37	558.3						
4-5	8.29	726.3	28.0	20336	0.50	21.6	15688	0.39
5-6	9.75	854.3	85.9	73384	1.79	78.0	66635	1.64
6-7	10.59	927.6	163.1	151292	3.69	155.6	144335	3.55
7-8	10.74	940.4	266.4	250523	6.10	262.1	246479	6.07
8-9	10.22	895.4	399.5	357712	8.72	398.9	357175	8.79
9-10	9.18	803.9	565.7	454766	11.08	565.4	454525	11.19
10-11	7.78	681.9	767.0	523017	12.74	761.4	519199	12.78
11-12	6.25	547.1	999.2	546662	13.32	985.1	538948	13.27
12-13	4.74	415.5	1254.5	521245	12.70	1237.5	514181	12.66
13-14	3.41	298.7	1500	448050	10.92	1500	448050	11.03
14-15	2.32	203.2	1500	304800	7.43	1500	304800	7.50
15-16	1.49	130.9	1500	196350	4.78	1500	196350	4.83
16-17	0.91	79.7	1500	119550	2.91	1500	119550	2.94
17-18	0.52	45.9	1500	68850	1.68	1500	68850	1.69
18-19	0.29	25	1500	37500	0.91	1500	37500	0.92
19-20	0.15	12.8	1500	19200	0.47	1500	19200	0.47
>20	0.08	7	1500	10500	0.26	1500	10500	0.26
Total	100.00	8760.20		4103738	100		4061965	100
Capacity factor:				*31.23%*			*30.91%*	

4.7 Practical considerations

It is interesting to note that the increase in energy yield by means of variable twist distribution will be more significant for "broad" wind regimes, i.e. regimes with a lower Weibull shape parameter (k). The value of k=2.39 which is used in this study, is relatively high. A common value for the Netherlands is k=2.0.
The improvement in energy yield with the application of torsional deformation also depends on the planform of the blade. For example, if the blade tip is 0.7 m instead of 1.0 m - e.g. to improve stall behaviour in favour of power limitation - the improvement in capacity factor would be 2.4 % (PVOPT, appendix D).
Additional theoretical improvement in power generation may be achieved because the blade twist is also adjusted due to wind speed variations in the rotor plane, particularly due to wind shear or other stochastic variations.

Another benefit is that, due to the higher initial blade twist angles in case of variable twist distribution, the starting torque on the rotor shaft is increased. For the Smart Rotor blade the torque at 5 m/s for conventional twist and variable twist distribution are T = 5450 Nm and 5993 Nm respectively. This increase of about 10 % is especially useful in reducing the required power for starting of the turbine from 0 to nominal rotor speed.

Concluding: The beneficial use of variable twist should be analyzed for each individual rotor design and type of control regulation, i.e. active or passive stall, positive pitch regulation, etc.
The typical elastic twist for optimum power generation of a constant speed rotor is that the outer 60 % of the Smart Rotor blade should twist towards stall, opposite to the inner part. The potential increase in energy yield in that case is estimated at several percentages, most significant for tapered blade planform and "broader" wind regimes.

5. OPTIMUM BENDING-TORSION FLEXIBILITY OF THE SMART ROTOR

5.1 Introduction

By combining the desired variation in twist distribution from chapter 4 with the discrete flatwise bending moments in the blade the bending-torsion flexibility is derived for optimum power generation below rated wind speed. § 5.2 gives the calculated bending moment lines for several wind speed. Also the definition of the effective chord length of a tapered blade element is explained in this paragraph. Next § 5.3 explains how the required flexibilities differ for each wind speed interval and how from those values the actual desired bending-torsion flexibilities h_{42} are determined.

5.2 Calculation of applied loadings

In addition to the determined twist variations in chapter 4, the flatwise bending moment distribution is determined for each wind speed interval for calculation of the required bending-torsion flexibilities.
With the use of the ECN computer programme "PHATAS-III" [ref. 13] the loading on the Smart Rotor blade are calculated for various (wind speed) conditions. The loads are:

$$\{f_{ij}\} = \begin{Bmatrix} T_z \\ M_x \\ M_y \\ M_z + D\,(x_{ba} - x_{sc}) \end{Bmatrix} \tag{25}$$

This preliminary design merely focuses on the bending-torsion flexibility of the blade. The induced torsional deformation due to axial force, edgewise bending and torsional moment (partially due to the offset between blade axis and shear centre) is neglected. The admission of this choice is discussed in chapter 8.3. So, the bending moment remains to induce torsional deformation.

By taking the twist and bending moment distribution at 5 m/s wind speed as references the desired values for h_{42} are calculated by using the increase in twist and bending moment going from 5 to 6, 5 to 7, ... and 5 to 13 m/s. Hence, for a certain wind speed interval the increase in flatwise bending along the span induces the torsional deformation as:

$$\Delta\theta = \frac{h_{24}^{*}}{t} \cdot \int_{r_i}^{r_i+\Delta r} \frac{\Delta M_x(r)}{c(r)^3}\, dr \tag{26}$$

Index i refers to the element borders, Δr is the element size.

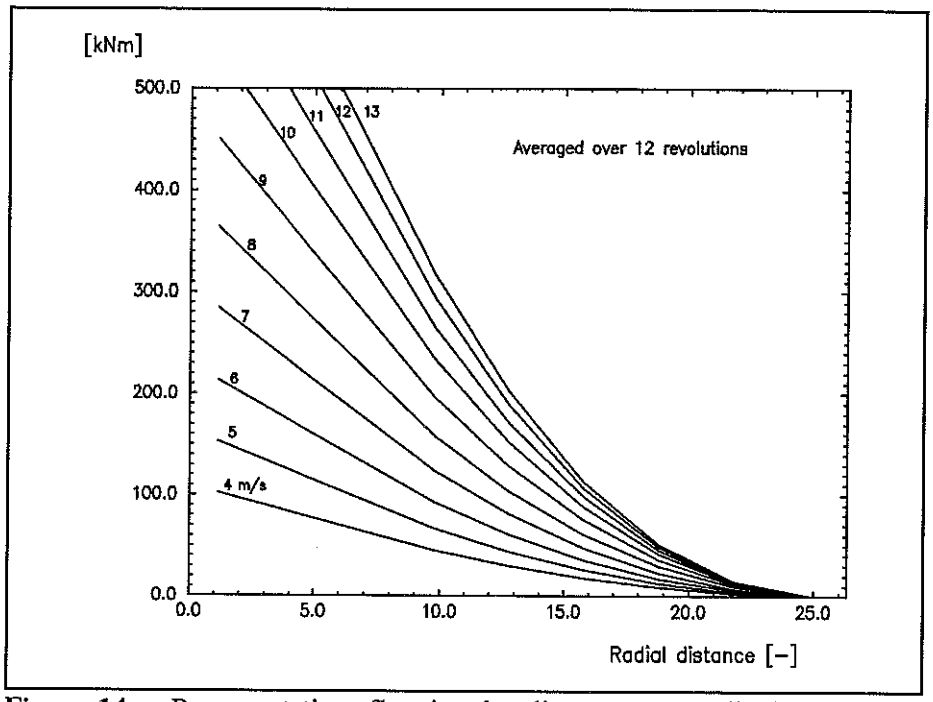

Figure 14: Representative flatwise bending moment distributions for Smart Rotor blade.

A useful simplification is formulated by taking the average bending moment in the element, thereby assuming a quasi linear distribution (equation 27):

$$\Delta\theta = \kappa_{xy} \cdot \Delta r = \frac{h_{24}^{*}}{t\bar{c}^{3}} \cdot \frac{\Delta M_i + \Delta M_{i+1}}{2} \cdot \Delta r \qquad (27)$$

$\bar{c}$ is the effective chord length of the tapered blade element, i.e. the weight average value which gives the same amount of induced torsional deformation when the element is considered to have a constant chord length as in (27). A specified derivation of the effective chord length is given in appendix E. The results show that for all elements of a tapered blade $\bar{c}$ is little more than the average value at the middle of the element.

radial position [m]	ΔM_1 [kNm]	ΔM_2 [kNm]	c_1 [m]	$c_{average}$ [m]	$\bar{c}$ [m]
9.8-12.8	304.7	201.2	2.725	2.568	2.574
12.8-15.8	201.2	118.3	2.411	2.254	2.319
15.8-18.8	118.3	57.2	2.097	1.941	1.956
18.8-21.8	57.2	18.5	1.784	1.627	1.654
21.8-24.8	18.5	1.4	1.470	1.314	1.368
21.8-26.3	1.4	0	1.470	1.235	1.375

Using the average value of the linearly increasing chord length of the blade element in equation (27) would thus overestimate the torsional deformation.

In practice the bending moment will vary due to higher order wind speed variations, tower influence, mass inertia loads, etc. Nevertheless, the use of the - over 12 revolutions - averaged flatwise bending moment as a parameter for the desired amount of coupling gives a good indication. Most of the higher order variations in bending moment are due to corresponding variations in wind speed, except for inertia loads, which are negligible when averaged over a longer time period.
More on qualitative analysis of the rotor stability is discussed in chapter 8.

5.3 Desired bending-torsion flexibility of the blade

For each blade element 8 combinations are found for ΔM_{flat} and $\Delta\theta_{desired}$; between 5 and 6 m/s, from 5 to 7, ... and from 5 to 13 m/s increase in wind speed. Evidently, only one value for bending-torsion flexibility (h_{42}) can be realised for each blade element.
From the 8 different optimum values the optimum bending-torsion flexibility of each element can be determined by weighing the relative energy capture of the *element* at every wind speed below rated. This involves quite some calculational work. As a useful simplification the weighed average value of h_{42} may very well be determined by taking the energy capture of the *whole blade* to weigh the importance of the desired optimum twist angle of the blade elements at every wind speed, i.e. assuming the performance of the whole blade to be representative for the individual blade elements. This procedure has been performed for the Smart Rotor blade.
The "aiming values" to be realised with the actual material properties are:

Desired bending-torsion flexibility h_{42}	
$r_{average}$ [m]	weighed value of h_{42} [rad/Nm^2]
11.3	1.9 E-8
14.3	1.5 E-8
17.3	3.9 E-8
20.3	1.3 E-7
24.05	7.1 E-7

Appendix F gives a more detailed description on the determination of the weighed average bending-torsion flexibilities.

Calculation of flatwise bending moment and twist is interdependent and should thus converge. By carrying out several iterative PHATAS calculations, without dynamic coupling between bending and torsion (see also § 8.4), it has been verified that this relation converges rather quickly with minor differences between initial and eventual values for twist and bending moment.

The applied accuracy in the determination of h_{42} (desired) is somewhat questionable, specifically the induced torsional deformation due to torsion deserves further attention (h_{44}).

6. MATERIALIZATION OF THE REQUIRED STIFFNESSES

6.1 Introduction

This chapter discusses the actual material design of the Smart Rotor blade.
For a quantitative analysis a spreadsheet computer programme has been developed, based on the cross section stiffness theory from chapter 3. The program structure is described in § 6.2. Next an investigation is made of the influence of the cross section geometry and the skin laminate on the cross section mechanical properties; § 6.3 and 6.4 respectively.
Lastly in § 6.5, the previously derived values in § 5.3 for the desired bending-torsion flexibility of the blade elements are compared with calculated material values.

6.2 Calculation tool for mechanical blade element properties

In order to carry out calculations a spreadsheet programme (EXCEL) has been written based on Karaolis' theory (chapter 3).
Several examples of the spreadsheet programme are included in the appendices I and L. The input parameters for the description of a blade element are:

1 its length in span direction (here typical 3.0 m, with exception of the tip section);
2 the effective chord length (chapter 5.2);
3 the definition of the defined aerodynamic profile of the blade element (such contour descriptions are given in terms of (x,y) coordinates in aerodynamic handbooks like from Abbott and Von Doenhoff [ref. 1]);
4 the extensional stiffness matrix [A] of the skin laminate (derived for any lay-up composition with classical lamination theory with the aid of the computer programme PLAMOR from TUD) and
5 the thickness of the laminate.

With the above described input, discrete stiffnesses, first moments of inertia, etc., are summarized along the contour and hence the stiffness matrix [H] and other derived mechanical properties of the blade elements are calculated.
The calculations of the spreadsheet have been compared with results from Karaolis' thesis for a NACA 0015 profile with anisotropic glass-, carbon-, and kevlar epoxy lay up (appendix G-1). Another comparison has been made with the ECN programme MATEC [Huitink, et. al., ref. 6] for calculations on NACA 636 - and NACA 646 profiles with orthotropic lay up (appendix G-2).

To investigate the influence of adjustments in profile geometry and/or skin laminate lay up on the cross section mechanical properties, expressions have been derived for the leading diagonal stiffnesses. The main stiffnesses if only an axial force, flatwise bending, edgewise bending and torsional moment are applied, are derived from the flexibility matrix (!) of the cross section as expressed in equations (31):

$$
\begin{aligned}
EA &= \frac{1}{h_{11}} \quad [N] & EA' &= \frac{1}{h^*_{11}} \quad [N/m^2] \\
EI_{flat} &= \frac{1}{h_{22}} \quad [Nm^2] & EI'_{flat} &= \frac{1}{h^*_{22}} \quad [N/m^2] \\
EI_{edge} &= \frac{1}{h_{33}} \quad [Nm^2] & EI'_{edge} &= \frac{1}{h^*_{33}} \quad [N/m^2] \\
GJ &= \frac{1}{h_{44}} \quad [Nm^2] & GJ' &= \frac{1}{h^*_{44}} \quad [N/m^2]
\end{aligned}
\tag{31}
$$

Definitions for h_{ij} are given in chapter 3.
Furthermore the induced torsion is expressed per unit axial strain due to bending and per applied unit bending moment as respectively (32):

$$
\begin{aligned}
B_s &= \frac{1}{y'_{max}} \frac{h^*_{24}}{h^*_{22}} \quad [rad] \\
B_m &= h^*_{24} \quad [m^2/N]
\end{aligned}
\tag{32}
$$

It has not been the aim of this study to carry out a material optimization. Nevertheless, an appropriate choice of the blade element mechanical properties has been made for further analysis.

6.3 Influence of geometry properties on the amount of coupling

The influence of the aerodynamic shape of the profile has been investigated for a unidirectional carbon epoxy laminated $[34]_s$, by respectively change in NACA series number, amount of camber and relative thickness.
Carbon fibre reinforced epoxy:

E_{11}= 130.5 GPa G_{12}= 6 GPa
E_{22}= 10.05 GPa υ_{21}= 0.263

i) A comparison between NACA 63 - and 64 series shows that a NACA 64 profile has a little bit higher value for induced torsion per axial strain. Other properties show negligible changes.

Influence of NACA series number; NACA 63 and 64 compared		
(arbitrary chord length)	NACA 63618	NACA 64618
B_s [-]	8.64	8.79
B_m [m^2/N]	3.08 E-9	3.07 E-9
EA' [N/m^2]	2.72 E10	2.71 E10
EI'_{flat} [N/m^2]	1.68 E8	1.69 E8
EI'_{edge} [N/m^2]	3.69 E9	3.69 E9
GJ' [N/m^2]	2.33 E8	2.34 E8

ii) Influence of camber, figures 15 and 16.

For a cambered profile the induced torsional deformation per unit axial strain (B_s) is less. It is though important to note that the effect will be much less when the y_{max} is related to the neutral axis. A better indication for the induced torsion per applied bending moment gives B_m; -5 % for the cambered profile. The smaller value for the axial stiffness (EA) for a cambered cross section is caused by inversion of the stiffness matrix. Specifically the non zero stiffness between axial force and bending curvature causes a smaller value of h_{11} for the cambered profile (H_{11}* is independent of camber). Also the difference in flatwise bending stiffness is most likely negligible when EI_{flat} for the cambered profile is related to the line through the neutral axis, the locus of points which encounter zero axial strain.

Influence of profile camber; NACA XX15 series and unidirectional $[18_{glass}]_s$ skin laminate.

(arbitrary chord length)	NACA 0015	NACA 4415 (% diff.)
B_s [-]	7.21	4.87 (-32.5)
B_m [m^2/N]	3.80 E-9	3.61 E-9 (- 5.0)
EA' [N/m^2]	4.98 E10	4.06 E10
EI'_{flat} [N/m^2]	1.50 E8	1.57 E8
EI'_{edge} [N/m^2]	4.29 E9	4.32 E9
GJ' [N/m^2]	1.05 E8	1.06 E8

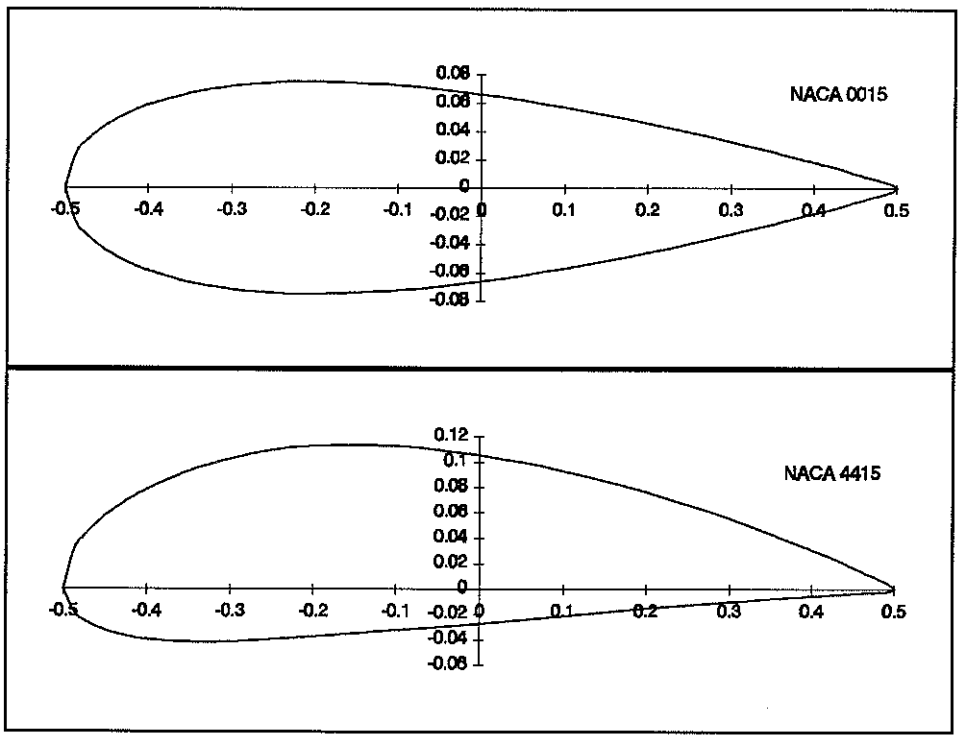

Figures 15 and 16: Contour of two NACA XX15 profiles.